A new cross section measurement of reactions induced by 3He-particles on a carbon target

A. Pichard, J. Mrazek, M. Assié, M. Hass, M. Honusek, G. Lhersonneau, Francois de Oliveira Santos, M.G. Saint-Laurent, E. Simeckova

EPJ manuscript No.
(will be inserted by the editor)

A new cross section measurement of reactions induced by ^{3}He-particles on a carbon target

A. Pichard[1], J. Mrázek[2], M. Assié[3], M. Hass[4], M. Honusek[2], G. Lhersonneau[1], F. de Oliveira Santos[1], M.-G. Saint-Laurent[1], and E. Šimečková[2]

[1] GANIL, CEA/DSM-CNRS/IN2P3, Caen, France

[2] Nuclear Physics Institute ASCR P.R.I., Řež, Czech Republic

[3] IPN, Université Paris-Sud - 11 - CNRS/IN2P3, Orsay, France

[4] Weizmann Institute, Rehovot, Israël

Received: date / Revised version: date

Abstract. The production of intense beams of light radioactive nuclei can be achieved at the SPIRAL2 facility using intense stable beams accelerated by the driver accelerator and impinging on light targets. The isotope ^{14}O is identified to be of high interest for future experiments. The excitation function of the production reaction ^{12}C(^{3}He, n)^{14}O was measured between 7 and 35 MeV. Results are compared with literature data. As an additional result, we report the first cross-section measurement for the ^{12}C(^{3}He, α+n)^{10}C reaction. Based on this new result, the potential in-target ^{14}O yield at SPIRAL2 was estimated: 2.4×10^{11} pps, for 1 mA of ^{3}He at 35 MeV. This is a factor 140 higher than the in-target yield at SPIRAL1.

PACS. 25.55.-e ^{3}H, ^{3}He and ^{4}He-induced reactions – 27.20.+n $6 < A < 19$

1 Introduction

A collaboration between GANIL (France), Soreq Nuclear Research Center and Weizmann Institute (Israël) has been formed in order to study the production options for intense light radioactive ion beams at the future SPIRAL2 [1] facility in the framework of the European FP7 Preparatory Phase of SPIRAL2 [2,3]. The short-lived (71 s) ^{14}O beam was identified to be of high interest for future experiments [4–7] and therefore options for its production have been studied in details. The reaction ^{12}C(^{3}He, n)^{14}O was chosen for production because a carbon target is able to sustain

Send offprint requests to: F. de Oliveira de Santos, e-mail francois.oliveira@ganil.fr

a very intense beam of ^{3}He. However, large discrepancies are observed in the various excitation functions available in the literature [8–11]. Moreover, above 10 MeV a strong difference appears between the integrated yield deduced from Ref. [11] and a thick target saturation activity measurement [12]. A single measurement using a thick target in order to fully stop the primary beam of ^{3}He could seem sufficient in order to estimate the yield for SPIRAL2. However, the beam power withstood by a target depends on primary beam intensity and energy. Good knowledge of the excitation function helps to choose the best primary beam energy, considering also beam power. Consequently, we decided to perform a new measurement of this cross section by an activation method. The production rate is deduced from the residual activity of thin carbon foils irradiated by the ^{3}He primary beam. Special attention has been devoted to the measurement normalisation. Apart from a standard current measurement, we counted the activity of aluminium and cobalt foils irradiated simultaneously by the primary beam. As a matter of fact, excitation functions for ^{27}Al(^{3}He, 2p)^{28}Al [13] and ^{59}Co(^{3}He, x) [14] - [20] reactions are reported in literature. A complementary results of this experiment is the first measurement of the excitation function of the ^{12}C(^{3}He, α+n)^{10}C reaction.

2 Experimental setup

The experiment took place at NPI (Nuclear Physics Institute), Řež, Czech Republic. The isochronous cyclotron U-120M can deliver ^{3}He^{2+} beams at energies up to 38 MeV. Measurements have been performed with two different beam energies: 38 and 24.5 MeV. Intermediate irradiation energies were obtained by means of energy degraders foils made of aluminium placed on a rack in front of the target. In figure 1, a scheme of the irradiation station is presented. The targets are composed of three stacked disks of 1 cm radius: a 3-μm thick Mylar disk, the thin carbon target (8.25mg/cm^{2}) and a 10-μm thick aluminium disk. The isotopic purity of the foils was 99.9 %.The carbon target wrapping prevents ^{14}O to escape in the volatile form C^{14}O. Moreover, the aluminium disk stops the reaction products having enough energy to leave the carbon target. A metallic plate located at the back of the target stopped the primary beam.

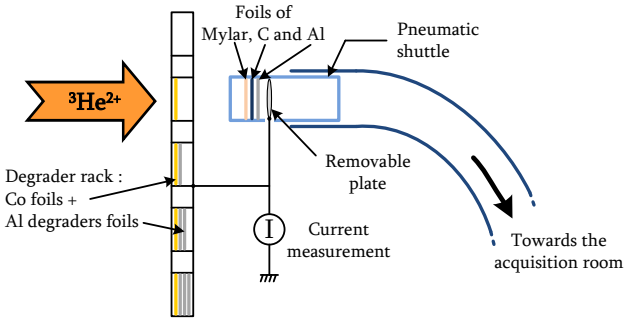

Fig. 1. Schematic view of the irradiation station.

The stacks were irradiated during 200 s, i.e. three times the ^{14}O lifetime (71 s), to reach near activity saturation. Then, the target was transported from the irradiation station to the low-background acquisition room via a pneumatic transport system. The detection set-up is shown in figure 2. The target was placed along the axis of a HPGe detector (53 % relative efficiency at 1.33 MeV). It was shielded with 2 cm of lead and 2 mm of iron in order to

reduce the flux of the very intense 511 keV gamma line (only 3% were still transmitted). The annihilation 511 keV γ-ray originates from the decays of ^{14}O, ^{11}C and ^{13}N reaction products. The cross-sections peak at 350 mb for the production of ^{11}C ($T_{1/2}$ = 20.38 m) and at 150 mb for the production of ^{13}N ($T_{1/2}$ = 9.96 m). Consequently, the ^{14}O cross-section was not determined using 511 keV-ray but using the 2312.6 keV, 718.4 keV and 1778.85 keV lines from ^{14}O, ^{10}C and ^{28}Al decays respectively. Three distances between the target and the detector were used in order to keep the counting rate at an acceptable level and the pile-up insignificant: 26.5 and 39.5 cm for thin targets and primary beam energy of 38 MeV and 24.5 MeV respectively, 106.9 cm for a thick target at 38 MeV. The counting rate was typically from 5.4 10^3 pps at the beginning down to less than 2.0 10^3 pps at the end of the radioactive cycle measurement, leading to an acceptation rate of 85 % at beginning to 95 % at the end. Corresponding rates for the 511 keV line were 250 and 100 pps. The detector was calibrated in energy and efficiency in the same configurations with ^{152}Eu and ^{90}Nb radioactive sources. A ^{90}Nb ($T_{1/2}$ =14.6 h) source was prepared by irradiating a 0.1 mm thick ^{nat}Zr foil by 15.3 MeV protons. The activity of ^{90}Nb was determined via its 1129 keV gamma line measured with another HPGe detector. That spectrometer was calibrated using point-like standards (^{152}Eu, ^{241}Am, ^{60}Co, ^{137}Cs and ^{133}Ba) supplied by the Czech Institute of Metrology. Combined uncertainties in the activity of the standards were between 0.3 % (^{241}Am) and 1.0 % (^{60}Co). Overall uncertainty of the ^{90}Nb activity was 3.5 %. The two main lines of ^{90}Nb are 1129 keV and 2319 keV with branching ratio and uncertainty of 92.7(0.5) % and 82 (3) % respectively [21]. This gave an efficiency point very close to the 2314 keV of interest. Each target counting lasted 300 s. Figure 3 shows a γ-ray spectrum from 35.3 MeV ^{3}He irradiation. The Co foils were counted until several weeks after irradiation due to the long life-time of some of the elements produced. Their counting rate being consequently lower, the detector was in a lead castle in order to limit the natural background. The distance between the target and the detector was 5.5 cm. There was no shielding between them. The Germanium counting rate was typically 50 pps.

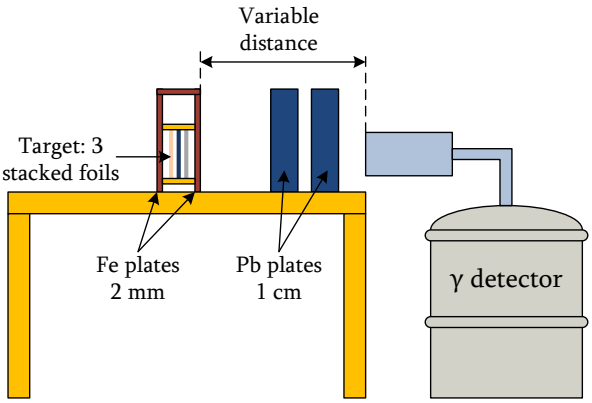

Fig. 2. Scheme of the acquisition setup placed in the low background room.

3 Data Evaluation

Basic nuclear data and threshold of the contributing reactions are collected in table 1. The 1238 keV ^{56}Co γ-line was not used because it was strongly contaminated by the room background. The number of incident particles was

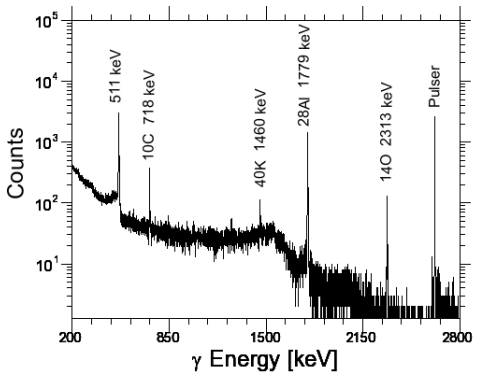

Fig. 3. γ-ray spectrum from 35.3 MeV ^{3}He irradiation on C/Al target.

obtained by real time measurement of the current collected on a metallic plate placed at the back of the target and on the degrader rack. Simultaneous irradiation of aluminium and cobalt foils by the beam allowed a check of this measurement:

− The cross section for ^{27}Al(^{3}He, 2p)^{28}Al is known to good accuracy [13]. The ^{28}Al (2.2 m) yield measured in the 10-μm aluminium foils placed at the back of the carbon target allowed us to calculate the ^{3}He integral intensity received by the target at each irradiation.

− The excitation functions of reactions induced by ^{3}He on cobalt being known too [14–20], a stack of 3 μm-thick cobalt foils placed on the degrader rack also allowed for checking the normalisation.

The cross-section uncertainties have been estimated by summing quadratically the uncertainties of the different contributing processes:

− The dead time of counting is monitored by a pulse generator. Its accuracy is always better than 1 %.

− Accuracies on branchings per decay of the monitored γ-rays, available from literature, are given in table 1.

− The accuracy on the efficiency of the γ detector, including transmission through the lead plates, is the main contribution to the total error. It is estimated to be about 6 % for the 2314 keV line of ^{14}O and the 1779 keV line of ^{28}Al. For the long counting of cobalt foils it is 10 % and about 25 % for the 718 keV line of ^{10}C.

− The number of target atoms in each disk is obtained by weighting. The accuracy is about 3 % for the aluminium and carbon disks and about 10 % for the thinner cobalt foils.

− The accuracy of the primary beam intensity is estimated to be 5 % from the current measurement device. It is confirmed by the evaluation of activity generated by the beam in Aluminium foils, see section 4.4.1.

4 Results

Table 2 shows the measured cross-sections obtained for the ^{12}C(^{3}He, n)^{14}O and ^{12}C(^{3}He, α+n)^{10}C reactions and for the ^{27}Al(^{3}He, 2p)^{28}Al monitor reaction. Each target was irradiated and counted twice (three times at 35.3 MeV) to check for consistency. The values listed as σ give the measured cross-section for each irradiation, which are subsequently combined to obtain the resultant mean value σ_r. The energy degradation ΔE inside the target and the mean primary beam energy $< E >$ were calculated with the code LISE++ [22] using the Ziegler [23] low-energy model for both C and Al foils. A measurement with a car-

Table 1. Investigated nuclear reactions induced in C, Al and Co by ^{3}He particles irradiation

Foil	Isotope	Half-life	E_γ (keV) [21]	I_γ (%) [21]	Reactions	Threshold (MeV)
^{12}C	^{14}O	70.61 s	2312.6	99.388(11)	^{12}C(^{3}He, n)^{14}O	1.4
	^{10}C	19.26 s	718.4	100.	^{12}C(^{3}He, α+n)^{10}C	14.1
					^{12}C(^{3}He, d+t)^{10}C	36.1
					^{12}C(^{3}He, n+p+t)^{10}C	38.9
					^{12}C(^{3}He, ^{3}He+2n)^{10}C	39.8
^{27}Al	^{28}Al	2.24 m	1778.85	100	^{27}Al(^{3}He, 2p)^{28}Al	0.
^{59}Co	^{60}Cu	23.7 m	826.4	21.7(11)	^{59}Co(^{3}He, 2n)^{60}Cu	5.3
			1791.6	45.4(23)		
	^{61}Cu	3.33 h	283.0	12.2(22)	^{59}Co(^{3}He, n)^{61}Cu	0.0
			656.0	10.8(20)		
	^{56}Co	77.23 d	846.8	99.94(3)	^{59}Co(^{3}He, 2n+α)^{56}Co	10.3
			1037.8	14.17(13)	^{59}Co(^{3}He, 2t)^{56}Co	22.2
					^{59}Co(^{3}He, n+d+t)^{56}Co	28.8
					^{59}Co(^{3}He, 2n+p+t)^{56}Co	31.1
					^{59}Co(^{3}He, 3n+^{3}He)^{56}Co	31.9
	^{57}Co	271.7 d	122.1	85.60(17)	^{59}Co(^{3}He, α+n)^{57}Co	0.
			136.5	10.68(8)	^{59}Co(^{3}He, d+t)^{57}Co	16.8
					^{59}Co(^{3}He, n+p+t)^{57}Co	19.2
					^{59}Co(^{3}He, ^{3}He+2n)^{57}Co	20.0
					^{59}Co(^{3}He, n+2d)^{57}Co	23.4
					^{59}Co(^{3}He, 2n+p+d)^{57}Co	25.8
					^{59}Co(^{3}He, 3n+2p)^{57}Co	28.1
	$^{58m+g}$Co	70.86 d	810.8	99.45	^{59}Co(^{3}He, α)^{58}Co	0.
					^{59}Co(^{3}He, p+t)^{58}Co	10.2
					^{59}Co(^{3}He, ^{3}He+n)^{58}Co	11.0
					^{59}Co(^{3}He, 2d)^{58}Co	14.4
					^{59}Co(^{3}He, n+p+d)^{58}Co	16.7
					^{59}Co(^{3}He, 2n+2p)^{58}Co	19.1

Table 2. Measured cross-sections for the ^{12}C(^{3}He, n)^{14}O, ^{12}C(^{3}He, α+n)^{10}C and ^{27}Al(^{3}He, 2p)^{28}Al reactions

^{12}C	^{27}Al	^{12}C(^{3}He, n)^{14}O		^{12}C(^{3}He, α+n)^{10}C		^{27}Al(^{3}He, 2p)^{28}Al	
<E> / ΔE (MeV)	<E> / ΔE (MeV)	σ (mb)	σ_r (mb)	σ (mb)	σ_r (mb)	σ (mb)	σ_r (mb)
7.2 / 4.1	4.2 / 1.7	19(2)	18(2)	-	-	24(2)	23(2)
		17(2)		-		23(2)	
14.4 / 2.4	12.8 / 0.8	7.2(7)	7.3(7)	-	-	184(15)	186(15)
		7.4(7)		-		187(15)	
18.0 / 2.0	16.7 / 0.7	5.6(6)	5.5(6)	-	1(1)	274(22)	265(22)
		5.4(6)		1(1)		255(42)	
20.0 / 1.9	18.8 / 0.6	3.9(4)	3.8(4)	2(1)	1.9(7)	217(18)	221(18)
		3.8(4)		1.8(7)		224(18)	
20.6 / 1.8	19.4 / 0.6	3.8(4)	3.8(3)	2.2(7)	2.4(7)	222(18)	227(18)
		3.8(4)		3(1)		232(19)	
26.3 / 1.5	25.3 / 0.5	3.0(3)	3.0(3)	11(3)	11(3)	161(14)	160(13)
		3.1(3)		11(3)		158(13)	
28.3 / 1.4	27.4 / 0.5	2.5(3)	2.5(3)	11(3)	12(3)	131(11)	131(11)
		2.5(3)		12(3)		132(11)	
29.7 / 1.3	28.8 / 0.4	1.8(2)	1.8(2)	10(3)	10(3)	121(10)	120(10)
		1.8(2)		9(3)		120(10)	
34.9 / 1.2	34.1 / 0.4	1.6(2)	1.7(2)	13(4)	13(3)	97(8)	98(8)
		1.7(2)		13(4)		100(8)	
35.3 / 1.2	34.6 / 0.4	1.3(2)	1.3(2)	13(4)	12(3)	96(8)	96(8)
		1.3(2)		13(4)		95(8)	
		1.4(2)		11(3)		98(8)	
18 / 18	-	2.9(3)	2.9(3)	-	-	-	-
		2.9(3)		-			

bon target thick enough to fully stop the primary beam was done at 36 MeV. This measurement directly gives the thick target yield. The cross-section integrated over the whole energy range (and folded with stopping power) was also deduced and is presented on the last line of table 2 for comparison.

4.1 The ^{12}C(^{3}He,n)^{14}O cross-section

Figure 4 shows a comparison of our measurement with literature. Three authors report measurements at low energy (2 to 12 MeV). The shape and normalization of the excitation functions presented by Cirilov et al. [8] and by Hahn and Ricci [9] seem to be consistent. For [8], we used data from NNDC [21]. They show a 15 mb maximum at 5 MeV. We note that these values were modified compared to those of the original paper. The excitation function presented by Osgood *et al.* [10] has quite a similar structure but, while the absolute value is comparable for energies lower than 4 MeV, it then rises to reach a 35 mb maximum at 7 MeV. The only measurement at higher energies was done by Singh [11] who, however has normalized his values to those of Osgood *et al.* His excitation function decreases smoothly from 27 mb at 6 MeV to 12 mb at 30 MeV. Our only measurement at low energy (7 MeV) places sigma between the values given by Osgood *et al.*, on the one hand, and those given by Cirilov *et al.* and by Hahn and Ricci, on the other hand. At higher energies, our values are a factor 4 lower than those of Singh.

Figure 5 compares experimental and various TALYS[24] calculations. The dotted line shows the cross section from TENDL-09 [25,26], a nuclear data library which provides the output of the TALYS code calculated with TALYS default parameters. The peak observed at about 6 MeV corresponds to the compound nucleus contribution. In this work, we have forced the code to take into account only the contribution of the ground state since all the excited states of ^{14}O would decay by $^{14}O^* \rightarrow ^{13}N + p$ (instead by γ-rays). This calculation (thick line) eliminates the bump at 16 MeV, whose contribution is consequently attributed to ^{13}N + p channel. Increasing the number of discrete levels considered in Hauser-Feshbach decay and gamma-ray cascade increases the ground state population (long dashed line). In this configuration, our data at low energy are in rather good agreement with the simulations. Yet, the long tail observed at energies higher than 15 MeV is not well reproduced by the calculations. It could be due to an underestimation of the preequilibrium contribution using the default parameters of TALYS.

4.2 Thick target yield of ^{14}O

The thick-target yields are obtained by folding the energy loss of the primary beam in the target with the excitation functions of the ^{12}C(^{3}He, n)^{14}O reaction. Figure 6 shows a comparison of these yields with the target saturation activities measured by Nozaki and Iwamoto [12] (full dots).

The dashed line is calculated from the excitation function given by Singh [11]. As already mentioned in the introduction, it shows a strong difference with the in-target saturation activities measured by Nozaki and Iwamoto

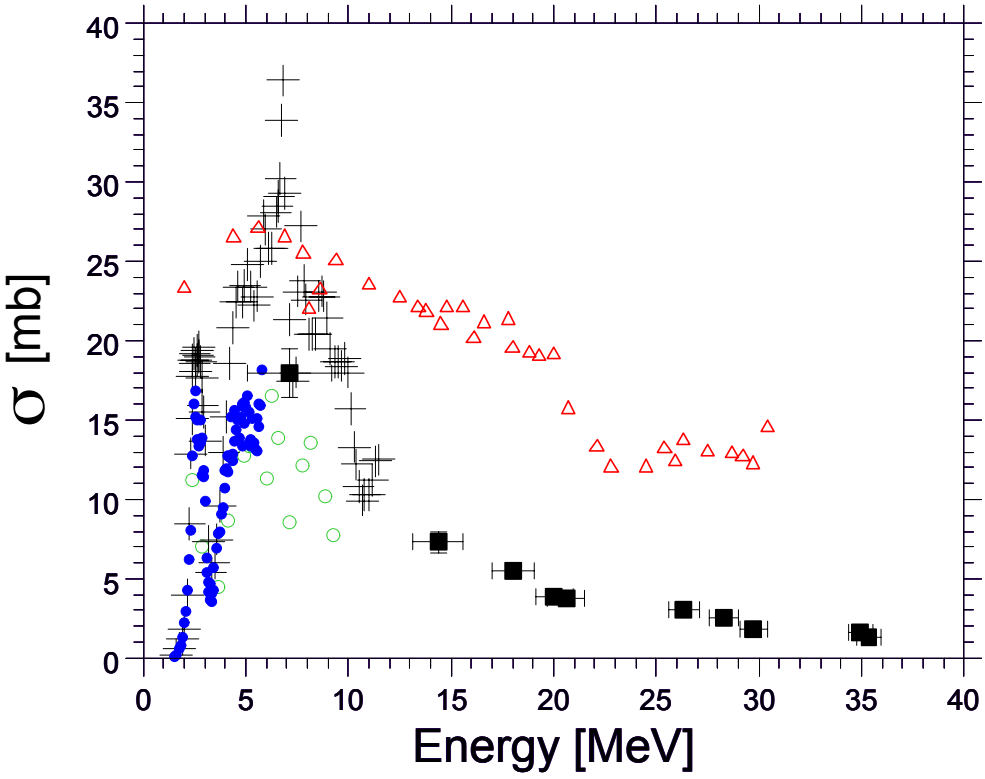

Fig. 4. Excitation functions for the ^{12}C(^{3}He,n)^{14}O reaction. ■: our data. ○: Hahn and Ricci. ┼: Osgood *et al.*. △: Singh. ●: Cirilov *et al.* modified by NNDC [21]

[12]. Solid lines are calculated with our data from 14.4 to 35.3 MeV and the limits resulting from the works of others at lower energy. The highest solid line is calculated with data from Osgood *et al.* for energies between 1.6 and 11.5 MeV. The lowest solid line is calculated with data from Cirilov *et al.* (1.55 to 5.76 MeV) and from Hahn and Ricci (6 to 12.2 MeV). The value calculated by integrating Singh's data up to 30 MeV, 5.7×10^{11} pps, could indicate he used a too high value for normalization. The target saturation activities (full dots) measured by Nozaki and Iwamoto are not consistent with the low-energy cross section measurements made by the other authors (lower and upper solid lines below 11 MeV). Our estimate of the in-target yield at SPIRAL2, read from the solid curves, ranges from 1.8 to 2.4×10^{11} pps for 1 mA of ^{3}He at 35 MeV. Another conclusion is that, using 20 MeV instead of 35 MeV (40% of target heating less) would result in a decrease by only a factor 2 in the yield.

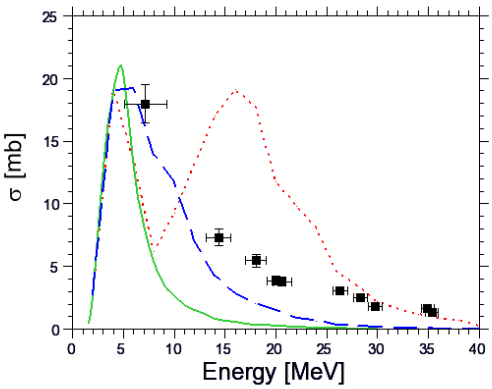

Fig. 5. Excitation functions for the ^{12}C(^{3}He,n)^{14}O reaction. ■: our data. Dotted line: TENDL-09 data base calculated with TALYS using default parameters. Solid line: population of the ^{14}O ground state only, calculated with TALYS and default parameters. Long dashed line: the same but calculated with larger number of discrete states considered in all nuclei.

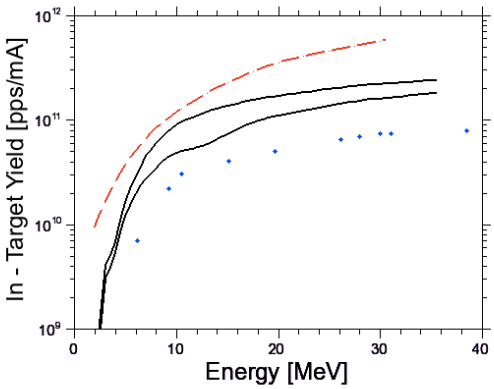

Fig. 6. Comparison of the thick target production yields for the ^{12}C(^{3}He,n)^{14}O reaction as a function of the primary beam energy. Dashed line: Singh. Solid lines: lower and upper estimates using our and combined data (see text for details). Full dots are Nozaki and Iwamoto target saturation activity measurements.

4.3 Cross-section for the production of ^{10}C

A by-product of this experiment is the measurement of the ^{10}C production cross-section. To our knowledge, this is the first report of experimental data for this reaction. In the energy range used, the reaction mainly contributing to the production is ^{12}C(^{3}He, α+ n)^{10}C (see the threshold value in table 1). In figure 7, they are compared with values given by TENDL-09. The measured cross section is zero for the lowest energies and starts to increase at about 18 MeV. This is due to the fact that the threshold of the ^{12}C(^{3}He,a+n)^{10}C reaction is equal to 14 MeV. The cross section reaches about 12 mb at the highest energy; this corresponds to the maximum of the compound nucleus contribution. The others channels start to be opened only above 36 MeV for the (^{3}He, d+t) channel and 39 MeV for channels (^{3}He, n+p+t) and (^{3}He, 2n+^{3}He). As for ^{14}O, we have forced the code TALYS to take into account only the contribution of the ground state and of the first discrete excited state since all the other excited states are known to be unbound for proton emission. The shape is well reproduced but not the normalisation. Increasing the number of discrete levels considered in Hauser-Feshbach decay and gamma-ray cascade also increases the ground state population (long dashed line), reducing the normalisation disagreement.

4.4 Monitor reactions

Special care was taken for the normalisation. For this goal, aluminium and cobalt foils were irradiated simultaneously with the targets to monitor the primary beam intensity.

4.4.1 Aluminium foils

The aluminium foil was the last disk of the target stack. A part of ^{28}Al produced via ^{27}Al(^{3}He, 2p)^{28}Al had enough kinetic energy to escape from the 10 μm-Al disk. This fraction was calculated with the ISOL Catcher utility [27] of the code LISE++. This fraction depends on the primary beam energy. At 34.6 MeV, it represents 23.5 % of the total production. In figure 8, our data (full squares) are compared to the measurement made by Frantsvog *et al.* (empty squares) and with the simulation data base TENDL-09 (dashed line). Frantsvog *et al.* used thicker targets so that their energy spread is larger than ours. Since we cannot compare directly their values to ours, we have interpolated our cross-section versus energy and subsequently integrated on the corresponding energy range. The resultant values are represented by full triangles on the graph. It appears that the agreement between our measurements and Frantsvog *et al.* data is good, comforting us in the validity of the normalization factor obtained by measuring the beam integrated charge.

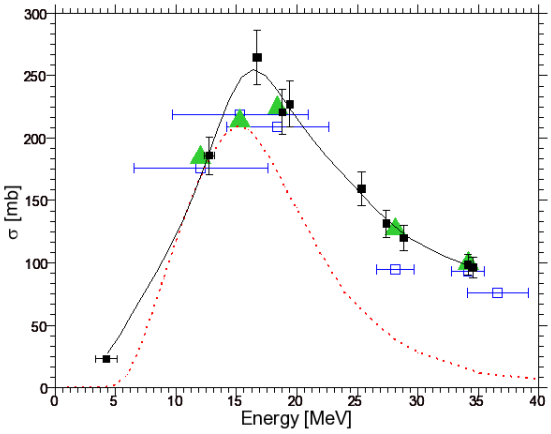

Fig. 8. Excitation function for the ^{27}Al(^{3}He, 2p)^{28}Al beam monitor reaction; ■: our data. □: Frantsvog *et al.*, ▲: our data averaged on the same energy spread for comparison with the ones of Frantsvog *et al.*. Dashed line: TENDL-09 data base. Solid line: a eye guide of our data.

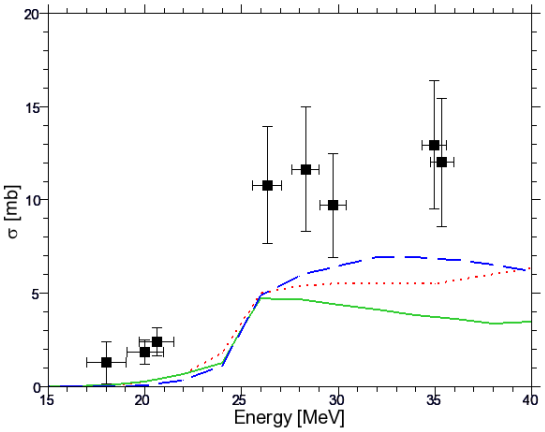

Fig. 7. Excitation functions for the ^{12}C(^{3}He, α+n)^{10}C reaction. ■: our data. Dotted line: TENDL-09 data base calculated with TALYS using default parameters. Solid line: ground state and first excited state calculated with TALYS and default parameters. Long dashed line: ground state with increasing the number of discrete levels considered with Hauser-Feshbach decay.

Table 3. Measured cross-sections σ (mb) for ^{3}He-induced reactions on ^{59}Co. Different values correspond to different Co foils

	<E> (MeV)	ΔE (MeV)	Our work	Mean	Literature (see text)
^{60}Cu	21.3	0.4	77(11)	77(11)	61.8(7.2) [14], 63.[15], 73.2(8.0)[16]
^{61}Cu	21.3	0.4	6.7(2.0), 7.6(2)	7.1(2)	4.4(1.1)[14], 5[15], 6.4(0.8)[16], 4.3(0.5)[17], 5.6(0.5)[20]
^{56}Co	21.3	0.4	9.4(2.0), 9.6(2.0)	9.5(2.0)	3.6(0.5)[14], 3.8[15], 6.9(0.5)[17], 6.2(0.5)[19], 2.4(0.3)[20]
	35.8	0.3	73(10), 64(9), 69(10)	69(6)	45.[15], 52.0(3.4) [17], 61(4)[19], 47.5(4.0) [20]
^{57}Co	21.3	0.4	116(14), 117(14)	116.5(10.0)	84.(10)[14], 67[15], 85(6) [17], 100(7) [19], 78(4) [20]
	35.8	0.3	50(8), 40(8), 44(8)	45(5)	20.4 [15], 30.4(2.1) [17], 37.8(2.9)[19], 31.6(1.9)[20]
^{58}Co	21.3	0.4	24(4), 24(4)	24(3)	16(2)[14], 16.4[15], 17.8(1.3)[17], 20(2)[19], 26.6(2.5)[20]
	35.8	0.3	289(39), 271(36), 284(39)	281(22)	192[15], 179.(13) [17], 268(20) [19], 128(8)[20]

4.4.2 Cobalt foils

Cobalt foils provided another set of cross-sections of the following reactions: ^{59}Co(^{3}He, 2n)^{60}Cu, ^{59}Co(^{3}He, n)^{61}Cu, ^{59}Co(^{3}He, x)^{56,57,58}Co, with x representing the various open channels (see table 1). The measured cross sections are shown in table 3. The proportion of reaction fragments leaving the Co foil is taken into account using the products recoil range measured by Nagame *et al.* [15] and Jastrzebski *et al.* [20]. It was determined that this proportion never exceeds 10 % at 21.3 MeV and 16 % at 38 MeV of the total production, in good agreement with factors calculated using the LISE++ code. Our measured cross sections were compared with those of Fenyvesi *et al.* [14], Nagame *et al.* [15], Szelecsényi *et al.* [16], Michel and Galas [17], Homma and Murakami [18], Kondratyev *et al.* [19] and Jastrzebski *et al.* [20]. The measured cross sections from the literature were interpolated and values corresponding to our energies are shown in table 3, with the exception of data from Homma and Murakami [18] which are already known to be wrong [14], [16]. Indeed all these published results are not in agreement, as demonstrated by the values given in the right column of table 3 which exhibit large discrepancies. Thus, the ratio between all these published values (except [18]) and our measured values fluctuates between

0.25 and 1.1. On the average, the published values are 30 % smaller than our values. We note that our results are scaled according to the primary beam intensity, these are absolute values. A part of the discrepancy could be ascribed to the thickness of the Co foils or to the estimate of products recoiling from the extremely thin Co targets. Moreover, beam intensity (100 nA) and irradiation time (200 s), optimized for ^{14}O and ^{28}Al, were not optimum for the decay measurements of the long lived ^{60,61}Cu and $^{56-58}$Co isotopes. It resulted in very low counting rates going from 0.001 pps up to 2.4 pps. In spite of the above mentioned limitations, if we scale our ^{12}C(^{3}He, n)^{14}O data according to our Co cross-sections, in no case we confirm the cross section of Singh (triangles in figure 4).

5 Outlook

The present measurement of the ^{12}C(^{3}He, n)^{14}O cross-section confirm a strong reduction of the cross section at energies higher than 6 MeV. For comparison, the TALYS code was used to predict the cross sections. Despite the fact it is not made for these light nuclei, predictions are in rather good agreement with the measurements. The shapes of the excitation functions are well reproduced. It seems that the preequilibrium contribution is often underestimated, but no correction was made to correct this fact.

An ^{14}O beam is currently available at GANIL within the SPIRAL1 facility. It is produced via the fragmentation of an ^{16}O 95 MeV/A primary beam impinging onto a graphite target. An intensity of 3.2×10^{5} particles per second after extraction and ionisation is available for experiments in an energy range from 3.2 up to 12.5 MeV/A [28]. With the new facility SPIRAL2, the intense ^{3}He (1 mA / 43.5 MeV) beam delivered by the LINAC driver offers opportunities to raise the available ^{14}O beam intensity. Based on our new result, we can estimate the potential in-target ^{14}O yield: 2.4×10^{11} pps, for 1 mA of ^{3}He at 35 MeV. This is 140 times higher than the in-target yield at SPIRAL1. Preliminary simulations of the thermal conditions did show that the maximal intensity the production target can withstand is indeed close to 1 mA. A production system is currently being designed at GANIL and simultaneously more precise thermal simulations will be carried out with the designed target.

6 Acknowledgement

We thank the Řež cyclotron and technical crew for delivering the ^{3}He beam and for the nice working conditions. We are also grateful to Dr. Lebeda for providing us the ^{90}Nb calibration source and to Dr. J. Kiener for helping us with the TALYS Code. This work has been supported by the IN2P3 - ASCR, by the European Community FP7 - Capacities - SPIRAL2 Preparatory Phase N^{o} 212692, and by the Région Basse Normandie for a PhD thesis (A.P.).

References

1. GANIL - SPIRAL2 - GANIL WEB PRO USERS, http://pro.ganil-spiral2.eu/.

2. G. Lhersonneau, A. Pichard, M. Saint Laurent, F. De Oliveira Santos, M. Hass, T.Y. Hirsh, *et al.*, Rapport Européen, WP7.1 Milestone 7.1.1, (2009).
3. M.G. Saint Laurent, A. Pichard, G. Lhersonneau, F. De Oliveira Santos, F. Pellemoine, P. Delahaye, et al., International Symposium on Exotic Nuclei (EXON), Sochi, Russian Federation (2009).
4. J.T. Burke, P.A. Vetter, S.J. Freedman, B.K. Fujikawa, W.T. Winter, Phys. Rev. C. 74 (2006) 025501-5.
5. M. Gaelens, J. Andrzejewski, J. Camps, P. Decrock, M. Huyse, K. Kruglov, et al., EPJ A 11 (2001) 413-420.
6. D.W. Bardayan, M.S. Smith, Phys. Rev. C. 56 (1997) 1647.
7. I. Stefan, F. De Oliveira Santos, M.G. Pellegriti, M. Angelique, J.C. Dalouzy, F. de Grancey, et al., International Conference-PROCON 2007, Lisbon (Portugal), AIP, (2007) 205-210.
8. S.D. Cirilov, J.O. Newton, J.P. Schapira, Nuclear Physics. 77 (1966) 472-476.
9. R.L. Hahn, E. Ricci, Phys. Rev. 146 (1966) 650.
10. D.R. Osgood, J.R. Patterson, E.W. Titterton, Nuclear Physics. 60 (1964) 503-508.
11. J. Singh, Nuclear Physics A. 155 (1970) 443-452.
12. T. Nozaki, M. Iwamoto, Radiochimica Acta. 29 (1981) 57-59.
13. D.J. Frantsvog, A.R. Kunselman, R.L. Wilson, C.S. Zaidins, C. Détraz, Phys. Rev. C. 25 (1982) 770.
14. A. Fenyvesi, F. Tárkányi, S.-. Heselius, NIM B. 222 (2004) 355-363.
15. Y. Nagame, Y. Nakamura, M. Takahashi, K. Sueki, H. Nakahara, Nuclear Physics A. 486 (1988) 77-90.
16. F. Szelecsényi, Z. Kovács, K. Suzuki, K. Okada, T. Fukumura, K. Mukai, NIM B. 222 (2004) 364-370.
17. R. Michel, M. Galas, Nuclear Physics A. 404 (1983) 77-92.
18. Y. Homma, Y. Murakami, Bull.of the Chemical Soc.of Japan. 50 (1977) 1251.
19. S. Kondratyev, Y. Lobach, V. Sklyarenko, Ukrainskii Fizichnii Zhurnal. 43 (1998) 5.
20. J.Jastrzebski, P.P. Singh, T. Mroz, S. E. Vigdor, M. Fatyga, H.J. Karwowski,Phis. Rev. C34 (1986) 34.
21. Nuclear database of NNDC, National Nuclear Data Center of Brookhaven, http://www.nndc.bnl.gov/
22. O. Tarasov, D. Bazin, NIM B. 266 (2008) 4657-4664.
23. U. Littmark, J.F. Ziegler, Handbook of range, distributions for energetic ions in all elements, Pergamon Press, 1980.
24. TALYS, http://www.talys.eu/home/.
25. TENDL-2009 - TALYS, http://www.talys.eu/tendl-2009/.
26. A.J. Koning, D. Rochman, to be published. JEFF-DOC 1310 (2009).
27. LISE++ : a simulation of fragment separators - Last modifications, http://groups.nscl.msu.edu/lise/changes.html.
28. Spiral beams - GANIL WEB PRO USERS, http://pro.ganil-spiral2.eu/users-guide/accelerators/spiral-beams.